Chemical Science

ROYAL SOCIETY OF CHEMISTRY

REVIEW

View Article Online
View Journal | View Issue

Cite this: *Chem. Sci.*, 2026, **17**, 4863

Beyond 800 nm: recent progress in high-performance near-infrared thermally activated delayed fluorescence based OLEDs

Shuo Li, Xiangyu Zhou, Lingjie Xu, Chao Yu, Junteng Liu,* Shouke Yan and Zhongjie Ren *

Received 20th November 2025
Accepted 2nd February 2026

DOI: 10.1039/d5sc09087c

rsc.li/chemical-science

Near-infrared (NIR) thermally activated delayed fluorescence (TADF) materials with emission peaks beyond 800 nm have attracted considerable attention owing to their potential applications in bioimaging, optical communication, and night-vision technologies. However, their development remains limited by the energy gap law, which leads to severe non-radiative decay and low external quantum efficiencies. In recent years, researchers have broken through these bottlenecks by employing various molecular design strategies, such as modulating charge-transfer characteristics and reducing the singlet–triplet energy splitting. These efforts have enabled the realization of efficient TADF emission extending into the deep-NIR region. In this review, we summarize recent advances in NIR-TADF emitters with emission maxima beyond 800 nm, focusing on their molecular design principles, photophysical properties, and device performance, and discuss future perspectives for achieving high-efficiency deep-NIR OLEDs.

1. Introduction

The near-infrared (NIR) region, encompassing wavelengths from 700 to 2500 nm, has been the focus of significant research interest owing to its utility in a range of applications such as bioimaging, optical communication, night-vision technologies, and information-secured displays.[1,2] Among various optoelectronic platforms, NIR organic light emitting diodes (OLEDs) stand out for their lightweight, flexibility, and low fabrication cost, holding great promise for next-generation display and sensing technologies.[3–6] However, conventional NIR emitters—such as metal complexes and conjugated polymers—typically suffer from low external quantum efficiencies (EQEs) due to inefficient exciton utilization and severe nonradiative losses in narrow-bandgap systems. This performance bottleneck arises from the well-known energy gap law, which dictates that non-radiative decay rates increase exponentially as the optical energy gap decreases.[7,8] Consequently, developing NIR emitters that can retain high luminescence efficiency at long wavelengths remains one of the most fundamental challenges in organic photonics.

In recent years, thermally activated delayed fluorescence (TADF) materials have emerged as a promising class of emitters capable of overcoming the exciton utilization limit inherent to traditional fluorescent systems.[9–16] By engineering a small

State Key Laboratory of Chemical Resource Engineering, Beijing University of Chemical Technology, Beijing 100029, China. E-mail: renzj@mail.buct.edu.cn

Shuo Li

Shuo Li is pursuing his PhD at the Beijing University of Chemical Technology under Prof. Zhongjie Ren. After receiving his M.S. in 2024 from the Sinopec Beijing Research Institute of Chemical Industry, his work now focuses on developing novel red-emitting TADF materials aimed at enhancing the efficiency of OLED devices.

Xiangyu Zhou

Xiangyu Zhou is a master's candidate at the Beijing University of Chemical Technology under the supervision of Prof. Zhongjie Ren. He obtained his bachelor's degree from the Qingdao University of Science and Technology in 2023. At present, his research focuses on TADF luminescent materials and related electronic devices.

singlet–triplet energy splitting (ΔE_{ST}), TADF materials enable efficient reverse intersystem crossing (RISC) from triplet to singlet states, allowing for the effective harvesting of both singlet and triplet excitons.[17] This metal-free mechanism theoretically affords 100% internal quantum efficiency (IQE) and has revolutionized visible-light OLEDs, achieving record-breaking efficiencies in blue, green, and red devices.[18–28] Extending this success into the NIR region, however, introduces new difficulties. The narrower energy gaps required for emission beyond 800 nm significantly enhance vibrational relaxation and suppress radiative transition rates, leading to decreased photoluminescence quantum yields (PLQYs).[29,30] Moreover, the strong charge-transfer (CT) character typically employed to reduce ΔE_{ST} often results in large reorganization energies and pronounced structural relaxation, further compromising emission efficiency.[31,32] Thus, balancing CT strength, molecular rigidity, and exciton dynamics has become essential for designing efficient NIR-TADF materials; however, many reported systems exhibit only spectral tails extending into the NIR region rather than true NIR emission. Consequently, TADF emitters with peak emission beyond 800 nm remain exceedingly rare and represent a highly valuable research target. Emission above 800 nm offers intrinsic advantages, including enhanced tissue penetration, reduced light scattering, and minimal background autofluorescence.[33] These advantages are critical for high-contrast bioimaging and also contribute to improved performance in optical communication, information security, and other optoelectronic applications, as shown in Fig. 1a.[34–40] Achieving efficient emission in this region, however, is fundamentally challenging due to narrow energy gaps and the constraints imposed by the energy gap law, which increase non-radiative decay.

Although TADF materials hold great promise for OLED applications, the development of NIR TADF OLEDs has progressed slowly, primarily due to the scarcity of efficient NIR emitters. As shown in Fig. 1, a typical NIR TADF OLED shares a layered device architecture similar to that of its visible-light counterpart, in which holes and electrons are injected from opposite electrodes, transported through the respective functional layers, and recombined within the emission layer to generate NIR electroluminescence. To address the intrinsic challenges associated with long-wavelength emission and mitigate efficiency loss, multiple molecular design strategies have been proposed. Nevertheless, NIR-TADF materials still suffer from pronounced efficiency and color-purity deficits compared with visible-light emitters, particularly when the emission wavelength extends beyond 900 nm toward the NIR-II region.

In this review, emission beyond 800 nm is referred to as deep-NIR, while the NIR-II region is defined as the region encompassing wavelengths longer than 1000 nm. We organize deep-NIR TADF emitters within a unified structural framework that correlates chemical structure modulation and condensed state engineering with deep-NIR emission behaviour (Fig. 2). As illustrated, the combined regulation of molecular structures and aggregation effectively narrows the energy gap and modulates excited-state processes, thereby enabling deep-NIR emission. In contrast, the present review specifically targets deep-NIR TADF systems, where EQE efficiency degradation becomes particularly severe and conventional design rules often fail. On this basis, recent progress in deep-NIR TADF materials is critically analyzed, and perspectives are also provided to

Junteng Liu

Liu Junteng is a professor at the School of Chemical Engineering, Beijing University of Chemical Technology. He obtained his PhD degree in 2009. His primary research interests cover chemical engineering processes and materials, and his recent research has been concentrated on TADF materials and devices.

Shouke Yan

Professor Shouke Yan received his MSc (1988) and PhD (1996) from the Changchun Institute of Applied Chemistry, Chinese Academy of Sciences. He worked at Dortmund University, Germany, during 1997–2001 and is now working at the Beijing University of Chemical Technology. His research is focused on the characterization and regulation of multiscale structures of polymers.

Zhongjie Ren

Professor Zhongjie Ren was awarded an MSc (2006) by the Changchun Institute of Applied Chemistry, Chinese Academy of Sciences. He received his PhD from the Institute of Chemistry, Chinese Academy of Sciences, in 2009. He was a visiting scholar at the University of Durham during 2014–2015. His research is focused on polymeric OLEDs, including thermally activated delayed fluorescence macromolecules for light-emitting materials, hosts and sensitizers.

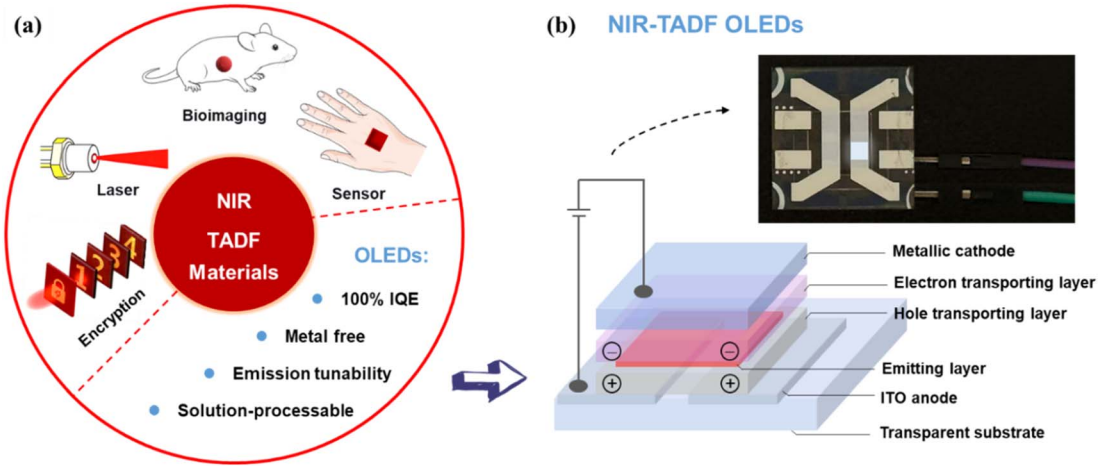

Fig. 1 Applications of NIR-TADF materials and corresponding OLED device architectures. (a) Summary of the various uses of NIR-TADF materials. (b) Device structure design for NIR TADF OLEDs and OLED images.

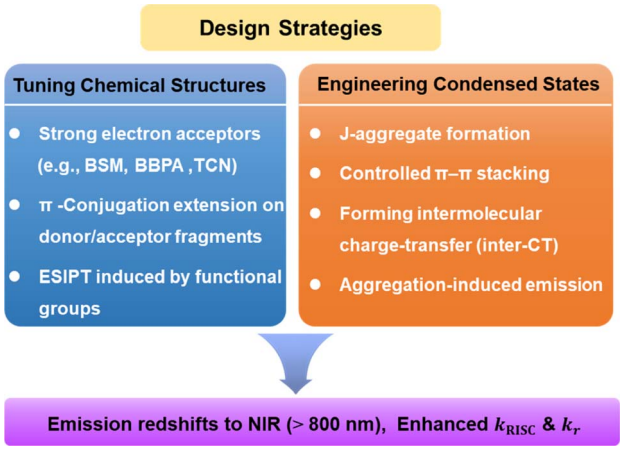

Fig. 2 Design strategies for deep-NIR TADF emission from the viewpoints of chemical structures and aggregate states.

guide the future development of high-efficiency deep-NIR OLEDs.

2. Molecular strategies, progress, and challenges

Guided by the framework in Fig. 2, we categorize the molecular strategies in this section into chemical structural tuning and condensed state engineering. This classification reflects their respective dominant roles in governing the photophysical processes of deep-NIR TADF systems.

2.1. Design principles for NIR-TADF emitters

To circumvent the limitations imposed by the energy gap law, precise molecular engineering is imperative. Conventional donor–acceptor (D–A) strategies focus on finely balancing the strength of donors and acceptors to optimize ICT while minimizing ΔE_{ST}. For long-wavelength TADF emitters, triphenylamine (TPA) and its derivatives are favored as donor units due to their strong electron-donating ability, high hole mobility, and readily tunable structures. On the acceptor side, strong electron-withdrawing groups—such as rigid planar heterocycles, quinoxaline derivatives, and boron-fluorine complexes—have been extensively employed to achieve redshifted emission, as illustrated in Fig. 3.[44–60]

In parallel to established methods, novel photophysical mechanisms have emerged as promising routes to mitigate the impact of the energy gap law. One such mechanism, excited-state intramolecular proton transfer (ESIPT), operates *via* a quasi-four-level system that concurrently boosts radiative transition rates, narrows emission bands, and induces marked redshifts, positioning it as a compelling approach for high-efficiency NIR emitters.[59] In addition, multi-resonance TADF (MR-TADF) designs based on B–N-fused polycyclic aromatic hydrocarbons exploit their alternating HOMO–LUMO profiles to suppress high-frequency vibrational quenching, thereby achieving narrowband and efficient deep-red to NIR TADF emitters.[41–43] Moreover, by modulating the CT character within these MR systems—a process enhanced by synergistic electron coupling—further emission redshift is achievable while preserving spectral narrowness. Collectively, although the current EL maxima of TADF molecules derived from these concepts remain below 800 nm, they furnish foundational insights and substantial scope for designing next generation NIR-TADF materials.

Consequently, the molecular design of NIR-TADF emitters requires a careful balance between minimizing ΔE_{ST} to enable efficient RISC and retaining fluorescence efficiency and spectral redshift, as summarized in Fig. 2. Here, we summarize representative single- and dual-donor TADF emitters reported in recent studies, some of which exhibit emission peaks beyond 800 nm (Fig. 4 and 5). These examples highlight diverse molecular strategies for extending TADF emission toward the deep-NIR region, while also underscoring the common efficiency challenges at longer wavelengths.

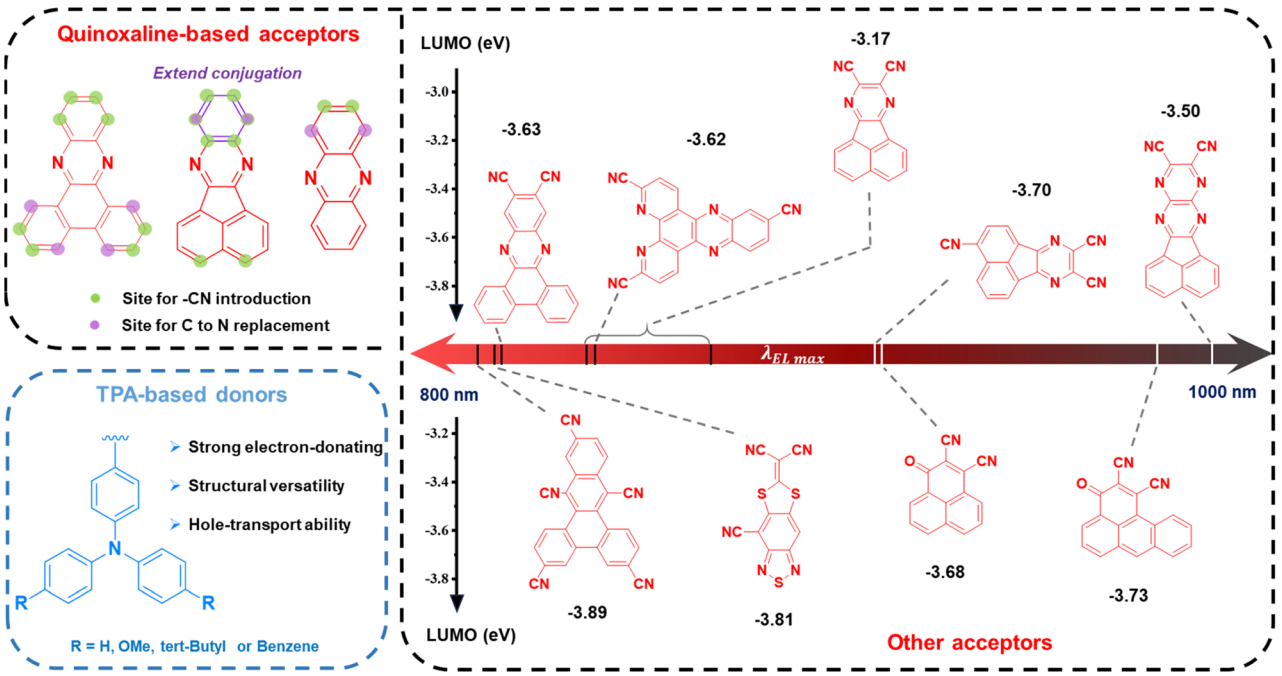

Fig. 3 Donor and acceptor structures, DFT-calculated LUMO energy levels of acceptors, and EL characteristics of representative deep-NIR TADF emitters.

2.2. Single-donor-based NIR-TADF molecules

Single-donor NIR TADF emitters benefit from simplified electronic coupling, enhanced structural rigidity, and clearer structure–property relationships, enabling effective ΔE_{ST} control while partially mitigating efficiency losses at long emission wavelengths. Under this design paradigm, a number of deep-NIR TADF emitters have been reported in recent years.

In 2019, Congrave, Bronstein and co-workers introduced a simplified molecular design strategy to achieve record-breaking NIR-TADF materials.[44] They developed the emitter CAT-1 (Fig. 4a) by strategically replacing a second electron donor in a reference D–A structure with a strongly electron-withdrawing cyano group, forming a simple D–A dyad. This design dramatically enhanced the intramolecular charge-

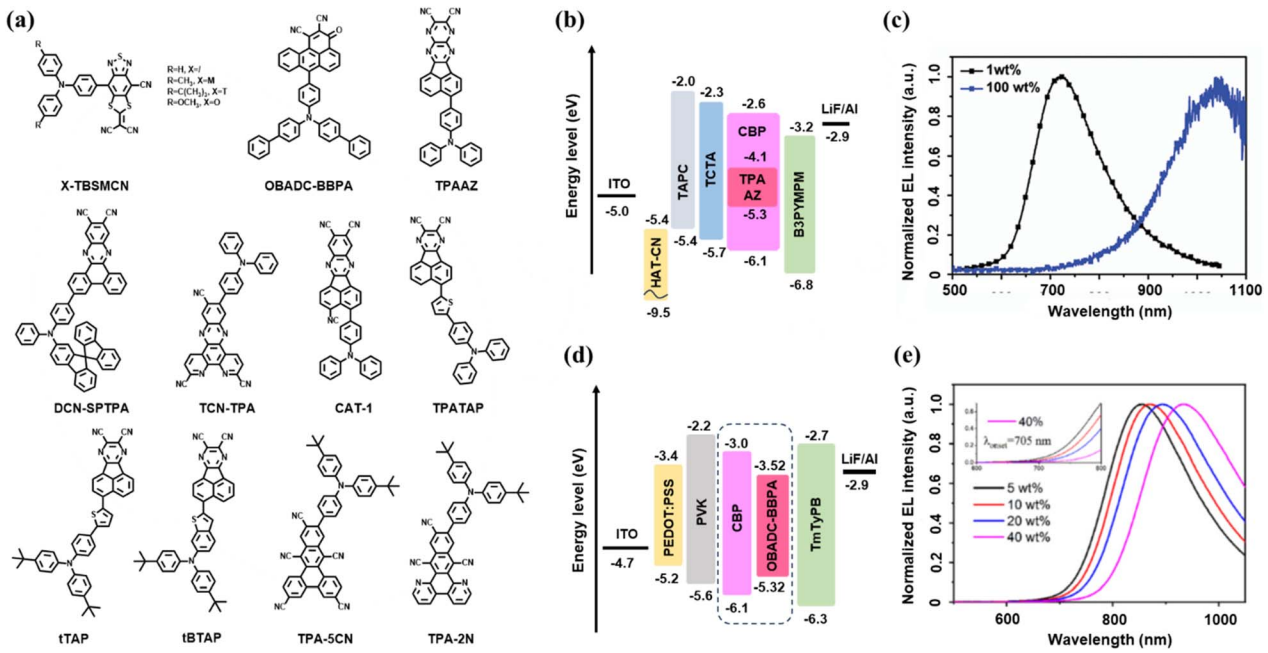

Fig. 4 Representative examples illustrating molecular design and device performance of single-donor deep-NIR TADF emitters. (a) Molecular structures of single-donor NIR-TADF emitters. (b) Device architecture and (c) EL spectrum of TPAAZ-based OLEDs (ref. 45). Copyright 2020 RSC. (d) Device architecture and (e) EL spectrum of OBADC-BBPA-based OLEDs (ref. 52). Copyright 2025 Elsevier B.V.

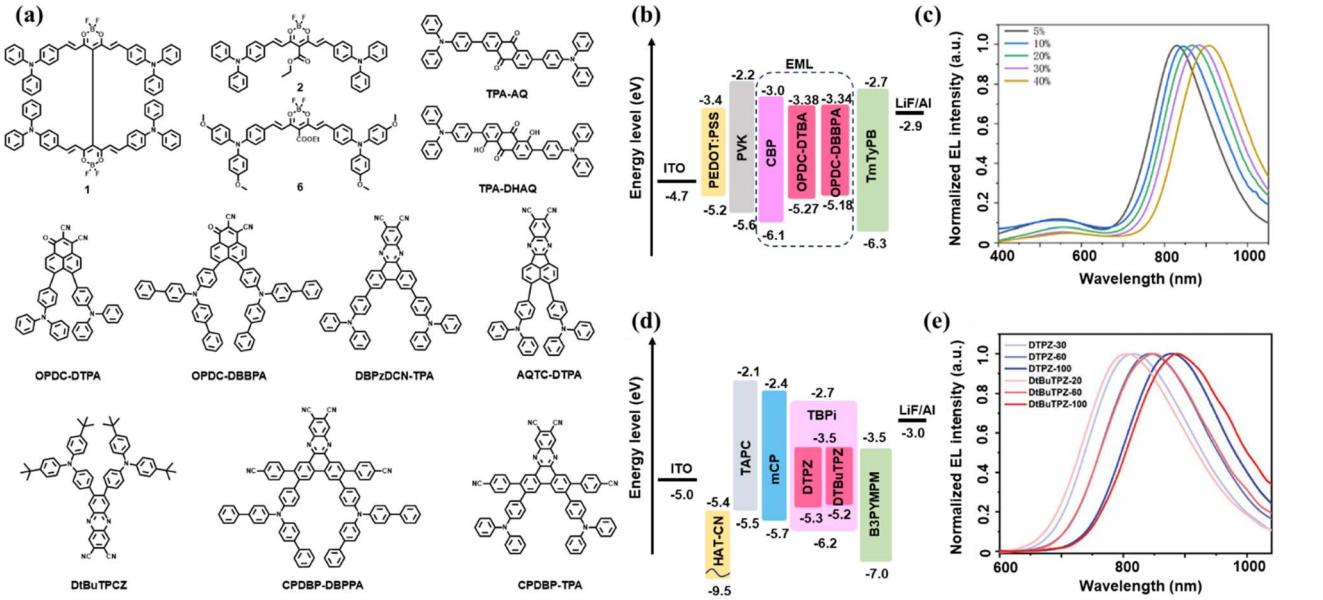

Fig. 5 Representative examples illustrating molecular structures and device performance of dual-donor deep-NIR TADF emitters. (a) Molecular structures of dual-donor NIR-TADF emitters. (b) Device architecture and (c) EL spectrum of the OPDC-DTPA and OPDC-DBBPA-based OLEDs (ref. 55). Copyright 2023 Wiley-VCH GmbH. (d) Device architecture and (e) EL spectrum of the DTPZ and DtBuTPZ-based OLEDs (ref. 56). Copyright 2023 Wiley-VCH GmbH.

transfer strength, resulting in a remarkably redshifted PL peak at 950 nm in a drop-cast neat film, which surpassed the previous record for TADF-capable emitters by over 100 nm. The electroluminescence potential of this design was confirmed in a preliminary undoped OLED, which exhibited an emission peak at 904 nm – the deepest red-shifted EL reported for a TADF device at that time. While the maximum EQE remained low at 0.019%, this work established the simple D–A dyad as a highly effective and synthetically accessible strategy for pushing TADF emission deep into the NIR region, opening new pathways for future material development.

In 2020, Liang, Qiao and colleagues pioneered a strategy utilizing intermolecular CT aggregates (CTAs) to achieve TADF in the NIR-II region.[45] They designed and synthesized the emitter TPAAZ (Fig. 4a), featuring an enhanced acceptor unit by embedding an additional electron-withdrawing pyrazine ring into the structure of a previously reported molecule. The PL emission exhibited a dramatic bathochromic shift with increasing doping concentration, culminating in a peak at 1009 nm in the neat film, which lies within the NIR-II biological window. Transient PL measurements of doped films confirmed prominent TADF character, with a delayed component ratio reaching up to 86%.

The OLED device structure fabricated using TPAAZ is shown in Fig. 4b. The corresponding non-doped OLED based on a TPAAZ neat film as the emitting layer successfully achieved electroluminescence in the NIR-II region, with a peak at 1010 nm, as shown in Fig. 4c. This device represents the first reported NIR-II TADF-OLED. While the maximum EQE remained low at 0.003%, this seminal work provides a groundbreaking and feasible strategy—leveraging CTAs to realize long-wavelength NIR-II TADF emission from organic materials, opening a new avenue for their application in advanced optoelectronics and bio-imaging.

Based on a newly developed electron-deficient acceptor BSM, Yu *et al.* introduced a family of D–A-type NIR emitters exhibiting both aggregation-induced emission (AIE) and TADF characteristics in 2022.[46] The strong electron-withdrawing ability of the BSM unit, coupled with a twisted molecular conformation, facilitates efficient ICT, minimizes ΔE_{ST}, and enables high PLQY in the solid state. The optimal emitter, TBSMCN (Fig. 4a), exhibits a solid-state emission peak at 820 nm with a PLQY of 10.7%. In non-doped, solution-processed OLEDs, TBSMCN achieved an exceptional EQE of 2.2% at 804 nm, representing state-of-the-art performance for metal-free NIR-OLEDs at the time. A further optimized ternary device incorporating a TADF sensitizer dramatically enhanced the EQE to 14.3% with an emission peak at 750 nm, setting a new benchmark in this spectral region.

Additional derivatives, including M-TBSMCN, T-TBSMCN, and O-TBSMCN (Fig. 4a), displayed progressively red-shifted emission at 854 nm, 868 nm, and 880 nm, with EQEs of 1.1%, 0.8%, and 0.3%, respectively. While TBSMCN offers the best balance between efficiency and wavelength, the entire series demonstrates the versatility of the BSMCN acceptor platform for developing efficient OLEDs operating across the deep-NIR range. This work underscores the powerful synergy between AIE and TADF strategies in achieving high-performance, solution-processable NIR electroluminescence.

Liang *et al.* reported the NIR-TADF emitter TCN-TPA (Fig. 4a) in 2023, which features a planar, multi-cyano acceptor unit combined with a triphenylamine donor.[47] This design promoted strong ICT and effective intermolecular through-space electronic coupling in the solid state, significantly

redshifting the emission while retaining a high PLQY of up to 30.5% at 730 nm in doped films. The molecule's rigid, linear structure also contributed to a high horizontal dipole ratio of 80%, enhancing optical outcoupling.

In fabricated OLEDs, TCN-TPA achieved widely tunable electroluminescence from 756 nm to 841 nm by varying the doping concentration. The devices delivered record-high EQEs of 2.4% at 802 nm and 1.1% at 841 nm, establishing a new benchmark for TADF-based OLEDs in the spectral region beyond 800 nm. This work successfully demonstrates the value of strong acceptor design and through-space coupling for developing high-performance deep-NIR TADF emitters.

Also in the prolific research year of 2023, Wang *et al.* demonstrated a distinct yet equally powerful strategy for high-performance NIR-TADF materials: terminal spiro-functionalization.[48] In contrast to the preceding approaches that focused on modulating electronic structures, their design centred on steric control of molecular packing. The emitter DCN-SPTPA (Fig. 4a), constructed by integrating a bulky spirobifluorene-based donor into a D–A framework, effectively suppressed concentration quenching by increasing intermolecular distances and steering the formation of favorable *J*-aggregates. This precise management of solid-state morphology enabled the material to retain near-unity PLQY (~100%) at 5 wt% doping and a high value of 82.4% even at 20 wt%, all while achieving significant bathochromic shifts.

The superior photophysical properties directly translated into record-breaking electroluminescence across the deep-red to NIR spectrum. Doped OLEDs based on DCN-SPTPA achieved exceptional EQEs of 36.1% at 656 nm, 29.3% at 688 nm, 28.2% at 696 nm, and 24.0% at 716 nm, outperforming the control emitter DCN-PhTPA by a factor of 1.3–1.4. Most notably, the non-doped device delivered efficient emission peaking at 800 nm with a state-of-the-art EQE of 2.61%, setting a new benchmark for NIR TADF OLEDs. This work establishes terminal spiro-functionalization as a highly effective steric-control strategy, complementing existing electronic-design paradigms for achieving both high efficiency and bathochromic emission.

By investigating the D–π–A molecule TPATAP (Fig. 4a), Xu *et al.* demonstrated in their 2024 study how strategic π-bridge regulation plays a crucial role in achieving highly efficient NIR emission in molecular aggregates.[49] They demonstrated that incorporating an electron-donating π-bridge, such as thienyl, is essential not only for inducing inter-CT character—which reduces ΔE_{ST} and activates TADF—but also for strongly coupling the inter-CT state with the bright ICT state. This electronic hybridization significantly enhances the radiative decay rate while effectively suppressing non-radiative decay, thereby overcoming the limitations imposed by the energy-gap law in the NIR region.

As a proof of concept, the thienyl-bridged emitter TPATAP achieved an exceptional solid-state PLQY of 18.9% at 788 nm in a doped film. Corresponding solution-processed OLEDs delivered record-high EQE among TADF NIR-TADF emitters, reaching 4.53% at 785 nm and 1.26% at 835 nm. This work establishes π-bridge engineering as a general and effective strategy for developing high-performance NIR-TADF materials *via* rational control of inter-CT and ICT interactions, opening avenues for advanced organic optoelectronic applications.

Dai and colleagues reported the D–π–A molecules tTAP and tBTAP (Fig. 4a) in their 2025 study, showcasing how strategic rigidification *via* a benzo[*b*]thiophene-fused donor design, following the established molecular engineering paradigm, leads to unprecedented performance in the critical beyond-800 nm region.[50] Unlike the previously reported π-bridge engineering approach that primarily modulates electronic coupling between inter-CT and ICT states, Dai's ring-fusion strategy created an integrated donor/π-bridge architecture that simultaneously enhances conjugation, minimizes dihedral distortion, and suppresses high-frequency molecular vibrations. This multi-faceted molecular design enabled the optimized emitter tBTAP to achieve exceptional solid-state PLQYs of 17.9% at 795 nm in doped films and 4.6% at 854 nm in neat films.

The resulting OLED performance set new benchmarks for long-wavelength NIR-TADF devices. The doped device achieved a record EQE of 3.64% at 796 nm, while the non-doped device reached 1.20% EQE at 867 nm—significantly advancing the efficiency frontier beyond 800 nm. More remarkably, the tBTAP-based non-doped OLED exhibited exceptional operational stability with a lifetime exceeding 2150 hours at 10 mA cm^{-2}, establishing the first longevity benchmark for practical NIR OLED applications. This work establishes the benzo[*b*]thiophene-fused donor architecture not merely as an alternative to π-bridge engineering, but as a superior platform for developing efficient and operationally stable NIR TADF materials toward real-world implementation.

Also in 2025, Hu and colleagues developed a novel NIR-TADF emitter, TPA-5CN (Fig. 4a),[51] by decorating a molecular framework with five strongly electron-withdrawing cyano groups, achieving an exceptionally low LUMO level of −3.80 eV. The high cyanidation density induced significant steric hindrance, leading to pronounced excited-state structural relaxation. This effect resulted in a record-long PL peak at 822 nm in toluene, though with a low PLQY of 7.7%. In contrast, the analogue TPA-2N, designed with less-hindered N atoms, exhibited a much smaller structural change and a higher solution PLQY of 65.9% at 698 nm.

When doped into a CBP host, the structural relaxation of TPA-5CN was suppressed, boosting the solid-state PLQY to 20% and blue-shifting the emission. The corresponding doped OLEDs delivered impressive electroluminescence in the NIR region, achieving maximum EQE of 4.52% at 766 nm and 2.56% at 796 nm for devices with 6 wt% and 10 wt% doping concentrations, respectively. These results rank among the best for doped NIR TADF OLEDs with emission peaks approaching 800 nm. This work demonstrates the effectiveness of leveraging excited-state structural relaxation for achieving long-wavelength NIR emission and provides valuable insights for molecular engineering in this challenging spectral region.

Zhou *et al.* developed OBADC-BBPA (Fig. 4a) through a molecular design combining an electron-deficient benzo[*de*]anthracene-2,3-dicarbonitrile core with a sterically hindered di([1,1′-biphenyl]-4 yl)amino donor in 2025.[52] The enlarged

conjugated skeleton and integration of multiple electron-deficient units resulted in a substantially lowered LUMO energy level, a consistently small ΔE_{ST} of 0.15 eV, and enhanced TADF characteristics. The OLED device structure fabricated with OBADC-BBPA is shown in Fig. 4d. The emitter displayed a PL peak at 1004 nm in the neat film (Fig. 4e), entering the NIR-II region, and achieved an EL peak at 933 nm in solution-processed OLEDs with an EQE of 0.073%—the highest value reported at that time for a NIR-II OLED within this spectral window. This work illustrates a rational molecular evolution from a single-acceptor to a multi-acceptor architecture, successfully extending emission further into the deep-NIR while retaining viable TADF performance.

2.3. Dual-donor-based NIR-TADF molecules

Dual-donor NIR TADF emitters provide stronger CT interactions and greater structural flexibility, facilitating deeper spectral redshift and small ΔE_{ST}. Guided by this strategy, multiple deep-NIR TADF emitters have been reported, albeit often accompanied by increased efficiency challenges at long wavelengths.

The pioneering work by Ye, Adachi, and co-workers in 2018 yielded the first solution-processable NIR-TADF emitter—a dimeric borondifluoride curcuminoid derivative that is recognized as a truly prototypical NIR TADF molecule named 1 (Fig. 5a).[53] The molecular design, which leveraged excitonic coupling between two curcuminoid-BF_2 units and incorporated a strong electron-withdrawing acetylacetonate group at the *meso* position, was strategically employed to achieve a substantial bathochromic shift in the emission profile. In doped thin films its PL peak exhibited a concentration-dependent redshift from 751 nm to 801 nm as the doping concentration in a CBP host was increased from 2 to 40 wt%, successfully pushing the emission into the deep-NIR region while retaining a measurable PLQY of 4% even at the highest concentration.

Particularly notable were its amplified spontaneous emission (ASE) characteristics in this spectral region. The material exhibited low-threshold ASE, with the peak wavelength tunable from 801 to 860 nm by varying the doping concentration. A remarkably low ASE threshold of 7.5 μJ cm^{-2} was achieved for the 2 wt% doped film. This work represented the first observation of ASE at wavelengths longer than 800 nm in an organic semiconducting film, marking a significant advancement for the development of NIR organic lasers.

In electroluminescent devices, the optimized OLED incorporating a 2 wt% doped emitting layer achieved a maximum EQE of 5.1% with an emission peak at 758 nm. At a significantly higher doping concentration of 40 wt%, the device exhibited a distinct bathochromic shift, reaching an emission maximum of 796 nm, albeit with a reduced EQE of 0.3%. While the most efficient device operated with an emission maximum situated just below 800 nm, this study successfully demonstrated the capability of the employed molecular engineering strategy to effectively extend the TADF emission—and, crucially, the lasing potential of these materials—well beyond the 800 nm threshold. These findings underscore the promising potential of this material design for high-performance NIR optoelectronic applications.

By integrating strong donor and acceptor units while leveraging through-space electronic coupling, Cheng *et al.* reported in 2022 a highly efficient NIR-TADF emitter named AQTC-DTPA (Fig. 5a).[54] The molecule features a large planar acenaphtho[1,2-*b*]quinoxaline core functionalized with three cyano groups as a strong electron-accepting unit, combined with twisted triphenylamine donors. This design not only promotes ICT but also enables strong intermolecular π–π interactions with a remarkably short stacking distance of 3.33 Å, as confirmed by single-crystal analysis. These through-space interactions effectively compensate for the interrupted intramolecular donor–acceptor electronic communication, significantly reducing the energy gap and enabling emission deep into the NIR region.

The emitter demonstrated concentration-dependent photophysical properties, with PLQYs ranging from 44.1% in toluene to 1.1% in neat films, while emission wavelengths redshifted from 636 nm to 878 nm. In optimized OLED devices, AQTC-DTPA achieved exceptional performance in the deep-NIR region, with maximum EQEs of 0.51% at 810 nm, 0.41% at 828 nm, 0.30% at 852 nm, and 0.23% at 894 nm – setting new efficiency records for TADF-based OLEDs in this spectral range. Furthermore, non-doped devices reached an emission peak at 910 nm with an EQE of 0.22%, demonstrating the effectiveness of this molecular design strategy for developing high-performance NIR-TADF emitters.

In 2023, Ma *et al.* reported a molecular design strategy utilizing a planar, strongly electron-deficient phenalenone-derived acceptor core, OPDC, which incorporates both carbonyl and dicyano groups to enhance electron-withdrawing capability and molecular rigidity.[55] By coupling this acceptor with diphenylamine (DTPA) and biphenylphenylamine (BBPA) donors, two D–A-type TADF emitters, OPDC-DTPA and OPDC-DBBPA (Fig. 5a), were synthesized. The strengthened acceptor and optimized D–A interaction led to efficient spatial HOMO–LUMO separation and small ΔE_{ST} (0.15 eV and 0.09 eV, respectively), facilitating k_{RISC}. As shown in Fig. 5b and c, the doped OLEDs exhibited EL peaks at 834 nm and 906 nm with maximum EQEs of 0.457% and 0.103%, respectively, representing some of the most efficient TADF-based OLEDs in this spectral region at the time.

Also in 2023, Xu *et al.* reported a novel molecular design strategy that synergistically integrates ICT to achieve highly efficient NIR-TADF beyond 800 nm.[56] Based on a phenazine-2,3-dicarbonitrile acceptor with a moderate LUMO level, they developed two emitters, DTPZ and DtBuTPZ (Fig. 5a), which retained appropriate ICT character while exhibiting unusually high oscillator strengths of 0.237 and 0.247, respectively. This design enabled strong ICT in aggregates through *J*-type packing with extensive van der Waals interactions but negligible π–π stacking. The resulting molecular arrangement significantly reduced the ΔE_{ST} to as low as 0.02 eV while retaining high radiative decay rates through effective electronic coupling between inter-CT and ICT states. As shown in Fig. 5d and e, the optimized devices demonstrated exceptional performance with

emission widely tunable from 807 nm to 886 nm. DTPZ-based OLEDs achieved record-high maximum EQEs of 2.28% at 817 nm and 0.57% at 877 nm in non-doped devices, along with remarkable radiance values up to 24.18 W Sr^{-1} m^{-2}. Similarly, DtBuTPZ-based devices reached 2.34% at 807 nm, representing state-of-the-art performance for NIR TADF OLEDs emitting beyond 800 nm. This work establishes the concerted ICT/inter-CT strategy as a promising approach to overcome the efficiency limitations imposed by the energy gap law in deep-NIR regions.

Building on the active research landscape of 2023, Jiang and colleagues introduced a molecular design strategy centered on a rigid, strongly electron-accepting core, 2,7-bis(4-cyanophenyl) dibenzo[*a*,*c*]phenazine-11,12-dicarbonitrile (CPDBP), to construct two efficient NIR-TADF emitters, CPDBP-TPA and CPDBP-DBPPA (Fig. 5a).[57] The strategic incorporation of cyanophenyl groups extended the π-conjugation, enhanced ICT, and promoted an optimally twisted donor–acceptor conformation. This rational design successfully balanced multiple key photophysical parameters, endowing the emitters with minimal ΔE_{ST} (0.01–0.05 eV), high PLQYs (80–85%), large horizontal dipole ratios and a remarkably fast k_{RISC} of 2.3–2.5 × 10^5 s^{-1} in doped films.

These outstanding photophysical properties translated into exceptional electroluminescence performance. The doped OLED based on CPDBP-TPA achieved a state-of-the-art maximum EQE of 30.3% at 646 nm, accompanied by notably low efficiency roll-off (EQE remaining at 21.8% at 100 cd m^{-2}). Even at a higher doping concentration that red-shifted the emission to 700 nm, the device retained a high maximum EQE of 19.3%. Furthermore, the non-doped device incorporating a CPDBP-TPA neat film delivered efficient NIR emission with a maximum EQE of 1.14% peaking at 850 nm—ranking among the best performances reported for deep-NIR TADF OLEDs. This work underscores the efficacy of such a molecular design paradigm in achieving high-performance NIR electroluminescence with minimal efficiency roll-off.

Based on the pursuit of efficient NIR-TADF materials, a 2025 study by D'Aléo *et al.* established a novel donor–acceptor–donor platform based on curcuminoid borondifluoride derivatives ($CurcBF_2$, Fig. 5a).[58] The key design innovation lies in a distinct TADF mechanism that relaxes the conventional requirement for minimal spatial HOMO–LUMO overlap. Instead, this system facilitates RISC *via* strong spin–orbit coupling between the singlet and higher-lying triplet states (*e.g.*, T_2), a pathway enabled by its unique electronic structure. Among the reported emitters, compound 6 demonstrated the ability to retain measurable solid-state PLQYs of 2% at 797 nm and 1% at 800 nm (at 15 and 20 wt% doping, respectively), successfully pushing efficient emission into the deep-NIR region. This molecular engineering directly yielded high-performance devices, with optimized OLEDs based on compound 4 (6 wt% in CBP) achieving a maximum EQE of 4.14% at 752 nm, while compound 6 (15 wt% in CBP) reached a NIR emission at 797 nm with an EQE of 0.99%. Despite the typical efficiency roll-off at high currents, these emitters also demonstrated outstanding low-threshold ASE tunable from 725 nm to 892 nm, with a threshold as low as 123 μJ cm^{-2}. This dual capability for efficient electroluminescence and ASE underscores the $CurcBF_2$ platform's significant potential for integrated NIR light-emitting and lasing applications.

Employing an innovative "two-in-one" molecular design, Che *et al.* successfully integrated TADF and ESIPT characteristics into a single emitter, TPA-DHAQ (Fig. 6a), in 2025.[59] As illustrated in Fig. 6a, this D–A–D structured molecule utilizes a 1,5-dihydroxyanthraquinone core that concurrently enables efficient TADF with a small ΔE_{ST} of 0.16 eV and introduces robust ESIPT *via* intramolecular hydrogen bonding. The dual-functional design promotes triplet exciton harvesting through RISC while establishing a four-level energy system conducive to population inversion, resulting in a substantial Stokes shift exceeding 150 nm. The synergistic interplay between TADF and ESIPT offers a novel pathway to suppress triplet accumulation and mitigate non-radiative decay, addressing pivotal challenges in the realization of NIR organic lasing.

When doped into polystyrene microsphere resonators, TPA-DHAQ achieves low-threshold NIR lasing at 820 nm with a threshold of 6.3 μJ cm^{-2}—among the best values reported for organic NIR lasers. By controlling resonator size, single-mode lasing at 796 nm was also achieved with a 13.4 μJ cm^{-2} threshold. The TADF-ESIPT system also provides excellent operational stability, retaining ≈80% of initial intensity after 580 minutes of continuous pumping. In the OLED structure shown in Fig. 6b, TPA-DHAQ delivers an EL peak at 745 nm and an EQE of 0.8% (Fig. 6c), highlighting its potential for future electrically pumped lasers. Although the emission remains below 800 nm, the synergistic TADF-ESIPT mechanism provides a novel design strategy for NIR-TADF materials. This work establishes a groundbreaking paradigm that simultaneously addresses the high threshold and poor stability of NIR organic

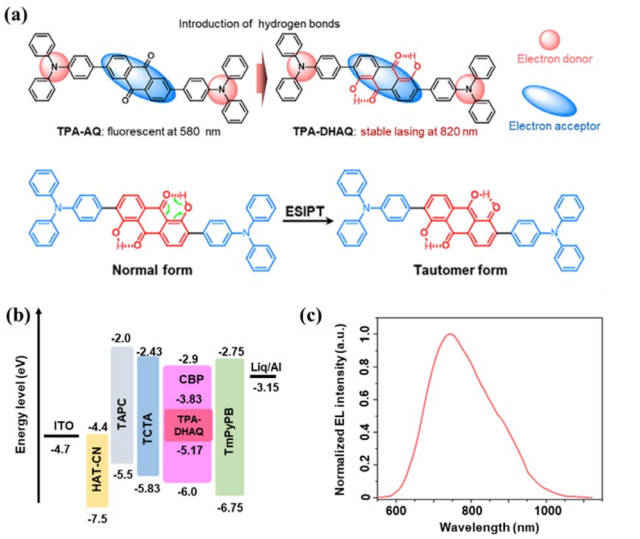

Fig. 6 Representative example illustrating ESIPT-assisted molecular design and device performance of NIR TADF emitters. (a) Molecular structures of TPA-AQ and TPA-DHAQ with an ESIPT scheme. (b) OLED device architecture of TPA-DHAQ. (c) EL spectrum of TPA-DHAQ. Reproduced from ref. 59. Copyright 2025 Wiley-VCH GmbH.

Table 1 Summary of the photophysical properties and OLED device performances of the TADF emitters covered in this review[a]

Emitter	Solid state λ_{PLmax}[a]/ PLQY/τ[b] [nm/%/μs]	Host	Device structure	λ_{EL} (nm)	EQE_{max} (%)	CE (cd A^{-1})	PE (lm W^{-1})	Radiance (mW Sr^{-1} cm^{-2})	Luminance (cd m^{-2})	Ref.
CAT-1	820[c]/2.0[c]/8[c]; 887[d]/0.18[d]/—[d]	Non-doped	ITO/TAPC (40 nm)/ CAT-1 (20 nm)/ TPBi (40 nm)/ LiF (1 nm)/ Al (100 nm)	904	0.019	—	—	0.1	—	44
TPAAZ	717[e]/10.7[e]/167.9[e]; 810[f]/4.2[f]/3.77[f]	Non-doped	ITO/HATCN (5 nm)/ TAPC (60 nm)/ TCTA (5 nm)/ TPAAZ (30 nm)/ B3PVMPM (60 nm)/ LiF (1 nm)/ Al (150 nm)	1010	0.003	—	—	—	—	45
TBSMCN	820/10.7/0.83	Non-doped	ITO/*m*-PEDOT:PSS (70 nm)/ TBSMCN (40 nm)/ DPEPO (10 nm)/ TmPyPB (50 nm)/ Liq (1 nm)/ Al (100 nm)	804	2.17	—	—	0.77		46
M-TBSMCN	852/4.6/0.99	Non-doped	ITO/*m*-PEDOT:PSS (70 nm)/ M-TBSMCN (40 nm)/ DPEPO (10 nm)/ TmPyPB (50 nm)/ Liq (1 nm)/Al (100 nm)	862	0.47	—	—	0.216		
T-TBSMCN	865/4.1/0.95	Non-doped	ITO/*m*-PEDOT:PSS (70 nm)/ T-TBSMCN (40 nm)/ DPEPO (10 nm)/ TmPyPB (50 nm)/ Liq (1 nm)/ Al (100 nm)	854	0.76	—	—	0.257		
O-TBSMCN	932/1.7/0.52	Non-doped	ITO/*m*-PEDOT:PSS (70 nm)/ O-TBSMCN (40 nm)/ DPEPO (10 nm)/ TmPyPB (50 nm)/ Liq (1 nm)/Al (100 nm)	876	0.022	—	—	0.01159		
TCN-TPA	730[g]/30.5[g]/50.1[g]; 803[h]/5.7[h]/9.6[h]	CBP	ITO (115 nm)/ MoO_3 (1 nm)/ TAPC (120 nm)/ CBP:30 wt% TCN-TPA (20 nm)/ B3PYMPM (80 nm)/ LiF (1 nm)/Al	802	2.4	0.06	0.03	3.5	—	47
		CBP	ITO (115 nm)/ MoO_3 (1 nm)/ TAPC (140 nm)/ CBP:30 wt% TCN-TPA (20 nm)/ B3PYMPM (80 nm)/ LiF (1 nm)/Al	802	2.4	0.06	0.03	3	—	
		CBP	ITO (115 nm)/ MoO_3 (1 nm)/ TAPC (115 nm)/ CBP:50 wt% TCN-TPA (20 nm)/ B3PYMPM (90 nm)/ LiF (1 nm)/Al	838	1.2	0.01	0.01	0.7	—	
		CBP	ITO (115 nm)/ MoO_3 (1 nm)/ TAPC (135 nm)/	841	1.1	0.01	0.01	0.7	—	

Table 1 (*Contd.*)

Emitter	Solid state λ_{PLmax}[a]/ PLQY/τ[b] [nm/%/μs]	Host	Device structure	λ_{EL} (nm)	EQE_{max} (%)	CE (cd A^{-1})	PE (lm W^{-1})	Radiance (mW Sr^{-1} cm^{-2})	Luminance (cd m^{-2})	Ref.
			CBP:50 wt% TCN-TPA (20 nm)/ B3PYMPM (90 nm)/ LiF (1 nm)/ Al							
		CBP	ITO (115 nm)/ MoO_3 (1 nm)/ TAPC (155 nm)/ CBP:50 wt% TCN-TPA (20 nm)/ B3PYMPM (90 nm)/ LiF (1 nm)/Al	841	1.1	0.01	0.01	0.4	—	
DCN-SPTPA	656[e]/99[e]/636[e]	Non-doped	ITO/HAT-CN (5 nm)/ TAPC (45 nm)/ TCTA (10 nm)/ mCP (10 nm)/ DCN-SPTPA (40 nm)/ TmPyPB (55 nm)/ LiF (1 nm)/ Al (120 nm)	800	2.61	—	—	—	—	48
TPATAP	834/4.1/5.1; 677[i]/67.1[i]/52.7[i]	Non-doped	ITO/HATCN (5 nm)/ TAPC (30 nm)/ mCP (5 nm)/ TPATAP (30 nm)/ B3PyMPM (60 nm)/ LiF/Al	835	1.26	—	—	0.47[j]	—	49
tTAP	865/1.8/5.49; 794[k]/9.7[k]/37.2[k]	Non-doped	ITO/HATCN (5 nm)/ TAPC (40 nm)/ mCP (5 nm)/ tTAP (20 nm)/ 46DCzPPM (6 nm)/ DPPyA (80 nm)/ LiF (1 nm)/ Al (120 nm)	857	0.37	—	—	0.724		50
tBTAP	854/4.6/5.18; 795[k]/17.9[k]/35.7[k]	Non-doped	ITO/HATCN (5 nm)/ TAPC (40 nm)/mCP (5 nm)/ tBTAP (20 nm)/ 46DCzPPM (6 nm)/ DPPyA (80 nm)/ LiF (1 nm)/Al (120 nm)	867	1.2	—	—	0.814		
TPA-5CN	751[l]/20.0[l]/4.34[l]	CBP	ITO/HAT-CN (10 nm)/ TAPC (50 nm)/ TCTA (10 nm)/ CBP:10 wt% TPA-5CN (20 nm)/ B4PyMPM (65 nm)/ Liq (2 nm)/ Al (100 nm)	796	2.56	0.01	0.01	—	3.38	51
OBADC-BBPA	871[f]/3.61[f]/11.26[f]	CBP	ITO/PEDOT:PSS (40 nm)/ PVK (5 nm)/ CBP:5 wt% OBADC-BBPA (20 nm)/ TmPyPB (40 nm)/ LiF (1.2 nm)/ Al (120 nm)	856	0.246	—	—	0.03491	—	52
		CBP	ITO/PEDOT:PSS (40 nm)/ PVK (5 nm)/ CBP:10 wt% OBADC-BBPA (20 nm)/ TmPyPB (40 nm)/	871	0.262	—	—	0.03862	—	

Table 1 (*Contd.*)

Emitter	Solid state λ_{PLmax}[a]/ PLQY/τ[b] [nm/%/μs]	Host	Device structure	λ_{EL} (nm)	EQE_{max} (%)	CE (cd A^{-1})	PE (lm W^{-1})	Radiance (mW Sr^{-1} cm^{-2})	Luminance (cd m^{-2})	Ref.
			LiF (1.2 nm)/ Al (120 nm)							
		CBP	ITO/PEDOT:PSS (40 nm)/ PVK (5 nm)/ CBP:20 wt% OBADC-BBPA (20 nm)/ TmPyPB (40 nm)/ LiF (1.2 nm)/ Al (120 nm)	892	0.172	—	—	0.03906	—	
		CBP	ITO/PEDOT:PSS (40 nm)/ PVK (5 nm)/ CBP:40 wt% OBADC-BBPA (20 nm)/ TmPyPB (40 nm)/ LiF (1.2 nm)/ Al (120 nm)	933	0.073	—	—	0.03606	—	
		Non-doped	ITO/PEDOT:PSS (40 nm)/ PVK (5 nm)/ OBADC-BBPA (20 nm)/ TmPyPB (40 nm)/ LiF (1.2 nm)/ Al (120 nm)	984	0.008	—	—	0.000439	—	
BF2 (1)	760[m]/45.2[m]/—[m]; 801[n]/4.1[n]/—[n]	CBP	ITO/PEDOT:PSS (45 nm)/ CBP:40 wt% 1 (80 nm)/ DPEPO (10 nm)/ TPBi (55 nm)/ LiF (1 nm)/ Al (100 nm)	796	0.3	—	—	—	—	53
AQTC-DTPA	878/1.10/9.70; 718[f]/19.10[f]/7.95[f]	CBP	ITO/HAT-CN (10 nm)/ TAPC (40 nm)/ TCTA (10 nm)/ CBP:60 wt% AQTC-DTPA (20 nm)/ PO-T2T (60 nm)/ Liq (2 nm)/Al (120 nm)	810	0.51	—	—	1.0224	—	54
		CBP	ITO/HAT-CN (10 nm)/ TAPC (40 nm)/TCTA (10 nm)/ CBP:70 wt% AQTC-DTPA (20 nm)/ PO-T2T (60 nm)/ Liq (2 nm)/ Al (120 nm)	828	0.41	—	—	0.5471	—	
		CBP	ITO/HAT-CN (10 nm)/ TAPC (40 nm)/TCTA (10 nm)/ CBP:80 wt% AQTC-DTPA (20 nm)/ PO-T2T (60 nm)/Liq (2 nm)/Al (120 nm)	852	0.3	—	—	0.4328	—	
		CBP	ITO/HAT-CN (10 nm)/ TAPC (40 nm)/TCTA (10 nm)/ CBP:100 wt% AQTC-DTPA (20 nm)/ PO-T2T (60 nm)/Liq (2 nm)/Al (120 nm)	894	0.23	—	—	0.31	—	
		Non-doped	ITO/HAT-CN (10 nm)/ TAPC (40 nm)/TCTA (10 nm)/AQTC-DTPA (30 nm)/TmPyPB (60 nm)/ Liq (2 nm)/Al (120 nm)	908	0.17	—	—	0.0915	—	

Table 1 (*Contd.*)

Emitter	Solid state λ_{PLmax}[a]/ PLQY/τ[b] [nm/%/μs]	Host	Device structure	λ_{EL} (nm)	EQE_{max} (%)	CE (cd A^{-1})	PE (lm W^{-1})	Radiance (mW Sr^{-1} cm^{-2})	Luminance (cd m^{-2})	Ref.
		Non-doped	ITO/HAT-CN (10 nm)/ TAPC (40 nm)/TCTA (10 nm)/ AQTC-DTPA (40 nm)/ TmPyPB (60 nm)/ Liq (2 nm)/Al (120 nm)	910	0.22	—	—	0.0961	—	
OPDC-DTPA	962/—/—; 814[o]/4.80[o]/8.00[o]	CBP	ITO/PEDOT:PSS (40 nm)/ PVK (10 nm)/ CBP:5 wt% OPDC-DTPA (30 nm)/ DPEPO (20 nm)/ TmPyPB (45 nm)/ LiF (1.2 nm)/Al (120 nm)	824	0.273	—	—	0.04586	—	55
		CBP	ITO/PEDOT:PSS (40 nm)/ PVK (10 nm)/CBP:10 wt% OPDC-DTPA (30 nm)/ DPEPO (20 nm)/ TmPyPB (45 nm)/ LiF (1.2 nm)/ Al (120 nm)	834	0.457	—	—	0.03794	—	
		CBP	ITO/PEDOT:PSS (40 nm)/ PVK (10 nm)/ CBP:20 wt% OPDC-DTPA (30 nm)/ DPEPO (20 nm)/ TmPyPB (45 nm)/ LiF (1.2 nm)/ Al (120 nm)	856	0.271	—	—	0.06761	—	
		CBP	ITO/PEDOT:PSS (40 nm)/ PVK (10 nm)/ CBP:30 wt% OPDC-DTPA (30 nm)/ DPEPO (20 nm)/ TmPyPB (45 nm)/LiF (1.2 nm)/Al (120 nm)	874	0.125	—	—	0.06994	—	
		CBP	ITO/PEDOT:PSS (40 nm)/ PVK (10 nm)/ CBP:40 wt% OPDC-DTPA (30 nm)/ DPEPO (20 nm)/ TmPyPB (45 nm)/ LiF (1.2 nm)/ Al (120 nm)	882	0.079	—	—	0.0597	—	
OPDC-DBBPA	1003/—/—; 828[o]/2.22[o]/6.00[o]	CBP	ITO/PEDOT:PSS (40 nm)/ PVK (10 nm)/ CBP:5 wt% OPDC-DBBPA (30 nm)/ DPEPO (20 nm)/ TmPyPB (45 nm)/ LiF (1.2 nm)/Al (120 nm)	830	0.354	—	—	0.03914	—	
		CBP	ITO/PEDOT:PSS (40 nm)/ PVK (10 nm)/ CBP:10 wt% OPDC-DBBPA (30 nm)/ DPEPO (20 nm)/ TmPyPB (45 nm)/	846	0.378	—	—	0.04305	—	

Table 1 (*Contd.*)

Emitter	Solid state λ_{PLmax}[a]/ PLQY/τ[b] [nm/%/μs]	Host	Device structure	λ_{EL} (nm)	EQE_{max} (%)	CE (cd A^{-1})	PE (lm W^{-1})	Radiance (mW Sr^{-1} cm^{-2})	Luminance (cd m^{-2})	Ref.
			LiF (1.2 nm)/ Al (120 nm)							
		CBP	ITO/PEDOT:PSS (40 nm)/ PVK (10 nm)/ CBP:20 wt% OPDC-DBBPA (30 nm)/ DPEPO (20 nm)/ TmPyPB (45 nm)/ LiF (1.2 nm)/Al (120 nm)	866	0.164	—	—	0.04486	—	
		CBP	ITO/PEDOT:PSS (40 nm)/ PVK (10 nm)/ CBP:30 wt% OPDC-DBBPA (30 nm)/ DPEPO (20 nm)/ TmPyPB (45 nm)/ LiF (1.2 nm)/Al (120 nm)	882	0.122	—	—	0.04815	—	
		CBP	ITO/PEDOT:PSS (40 nm)/ PVK (10 nm)/ CBP:40 wt% OPDC-DBBPA (30 nm)/ DPEPO (20 nm)/ TmPyPB (45 nm)/ LiF (1.2 nm)/ Al (120 nm)	906	0.103	—	—	0.04365	—	
DTPZ	880/2.1/3.09	TPBi	ITO/HATCN (5 nm)/ TAPC (30 nm)/mCP (5 nm)/ TPBi:30 wt% DTPZ (20 nm)/B3PyMPM (70 nm)/LiF (1 nm)/ Al (120 nm)	817	2.28	—	—	2.418	—	56
DTPZ		TPBi	ITO/HATCN (5 nm)/ TAPC (30 nm)/ mCP (5 nm)/ TPBi:60 wt% DTPZ (20 nm)/ B3PyMPM (70 nm)/ LiF (1 nm)/Al (120 nm)	846	1.29	—	—	1.765	—	56
		Non-doped	ITO/HATCN (5 nm)/ TAPC (30 nm)/mCP (5 nm)/DTPZ (20 nm)/ B3PyMPM (70 nm)/ LiF (1 nm)/Al (120 nm)	877	0.57	—	—	1.438	—	
DtBuTPZ	891/1.7/3.67	TPBi	ITO/HATCN (5 nm)/ TAPC (30 nm)/ mCP (5 nm)/ TPBi:20 wt% DtBuTPZ (20 nm)/ B3PyMPM (70 nm)/ LiF (1 nm)/Al (120 nm)	807	2.34	—	—	2.355	—	
		TPBi	ITO/HATCN (5 nm)/ TAPC (30 nm)/ mCP (5 nm)/ TPBi:60 wt% DtBuTPZ (20 nm)/ B3PyMPM (70 nm)/ LiF (1 nm)/Al (120 nm)	850	1.19	—	—	0.901	—	
		Non-doped	ITO/HATCN (5 nm)/ TAPC (30 nm)/mCP (5 nm)/DtBuTPZ (20 nm)/ B3PyMPM (70 nm)/	886	0.35	—	—	0.49	—	

Table 1 (*Contd.*)

Emitter	Solid state λ_{PLmax}[a]/ PLQY/τ[b] [nm/%/μs]	Host	Device structure	λ_{EL} (nm)	EQE_{max} (%)	CE (cd A^{-1})	PE (lm W^{-1})	Radiance (mW Sr^{-1} cm^{-2})	Luminance (cd m^{-2})	Ref.
CPDBP-TPA	829/—/—; 620[l]/85[l]/17.4[l]	Non-doped	LiF (1 nm)/ Al (120 nm) ITO/MoO_3 (5 nm)/ TAPC (50 nm)/TCTA (5 nm)/ CPDBP-TPA (20 nm)/ TmPyPB (60 nm)/ LiF (1 nm)/Al	850	1.14	0.013	0.0088	—	43	57
CPDBP-DBPPA	842/—/—; 628[l]/80[l]/12.0[l]	Non-doped	ITO/MoO_3 (5 nm)/ TAPC (50 nm)/ TCTA (5 nm)/ CPDBP-DBPPA (20 nm)/ TmPyPB (60 nm)/ LiF (1 nm)/Al	856	0.59	0.0063	0.003	—	13	
CucrcBF2 6	748[c]/11.6[c]/—	CBP	ITO/PEDOT:PSS/ CBP:20 wt% 6/DPEPO/ TPBI/LiF/Al	800	0.59	—	—	—	—	58
TPA-DHAQ	800/0.9/0.13; 780[c]/5.3[c]/10.2[c]	CBP	ITO/HAT-CN (10 nm)/ TAPC (40 nm)/TCTA (10 nm)/ CBP:10 wt% TPA-DHAQ (30 nm)/ TmPyPb (45 nm)/ Liq (2.5 nm)/ Al (100 nm)	745	0.8	—	—	—	—	59

[a] Conditions for photophysical and device measurements are indicated as follows: a, neat film; b, delayed fluorescence lifetime; c, 40 wt% in CBP; d, evaporated neat film; e, 1 wt% in CBP; f, 10 wt% in CBP; g, 9 wt% in CBP; h, 50 wt% in CBP; i, 1 wt% in TBPi; j, mW cm^{-2}; k, 60 wt% in RH; l, 3 wt% in CBP; m, 2 wt% in CBP; n, 40 wt% in CBP; o, 5 wt% in CBP.

lasers, opening a promising avenue toward practical organic laser diodes.

2.4. Theoretical design of NIR-TADF emitters

Guided by a strategic molecular design centered on the nitrogen-substituted polycyclic aromatic hydrocarbon (PAH) scaffold, Sahoo, Baryshnikov, and Ågren in their 2025 study conducted a comprehensive theoretical investigation into red and NIR-TADF emitters.[60] The study employed dibenzo[*a*,*c*] picene (DBP) as a foundational core, systematically introducing symmetric nitrogen atoms to create a series of electron-deficient acceptors (A1–A4). This nitrogen functionalization effectively stabilized the LUMO and narrowed the HOMO–LUMO energy gap. These engineered acceptors were then coupled with strong electron donors, namely dimethylcarbazole (DMCz) and dimethyldiphenylamine (DMDPA), *via para* or *ortho* linkages to construct 16 distinct D–A-type molecules. A key design insight was the role of the linking position: *ortho*-linked isomers consistently exhibited larger donor–acceptor dihedral angles, which proved crucial for achieving minimal ΔE_{ST}.

The theoretical calculations predicted outstanding performance metrics for the designed emitters. The higher-order nitrogen-substituted (4N) compounds exhibited exceptionally small ΔE_{ST} and high k_{RISC} up to 10^6 s^{-1}, confirming their strong potential for efficient TADF. Specific emitters were projected to achieve delayed fluorescence at distinct wavelengths: the *para*-linked compound B4 was predicted to emit at 670 nm, while the *ortho*-linked compounds D4 and D3 were forecasted for emission at 713 nm and 987 nm, respectively. This work establishes symmetric nitrogen doping and ortho-linked D–A architectures as powerful design strategies for developing efficient red and NIR-TADF emitters, providing a valuable theoretical roadmap for future synthetic exploration.

2.5. Device design principles for NIR TADF OLEDs

Despite the diversity of reported device architectures, the design of NIR TADF OLEDs generally follows a set of shared principles that aim to balance charge injection, exciton confinement, and optical efficiency at long emission wavelengths. Based on fabrication methods, these devices can be broadly categorized into vapor-deposited and solution-processed configurations, each with distinct yet related design considerations. The key photophysical parameters, device configurations, and optoelectronic performance of representative TADF emitters are compiled in Table 1, highlighting the intrinsic trade-off between emission wavelength and device efficiency in deep-NIR TADF OLEDs and general device-level considerations such as charge balance, exciton confinement, and suppression of non-radiative losses.

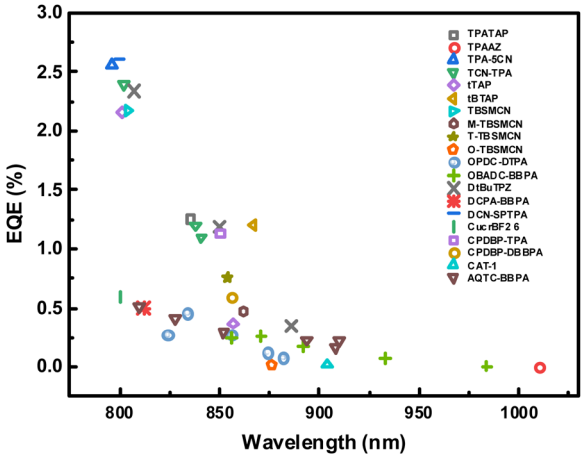

Fig. 7 EQE summary of the representative NIR TADF OLEDs.

For vapor-deposited NIR TADF OLEDs, efficient charge injection and transport are typically achieved using strong hole-injection and transport materials such as HATCN and TAPC, which help establish balanced carrier recombination in multi-layer architectures. In solution-processed NIR TADF OLEDs, greater emphasis is placed on interfacial engineering and film-forming properties. Conductive polymer layers such as PEDOT:PSS are commonly employed to improve hole injection and smooth the anode interface, while polymeric materials like PVK serve as hole-transporting or host matrices that support uniform film formation and morphological stability. Across both fabrication routes, wide-bandgap host materials (*e.g.*, CBP or TBPi) play a central role in device design. These hosts are widely adopted to ensure favorable energy-level alignment and effective exciton confinement within the emissive layer, which is particularly critical for NIR emitters with small bandgaps that are prone to charge leakage and non-radiative losses.

Fig. 7 summarizes the EQEs of representative NIR TADF OLEDs as a function of emission wavelength, clearly illustrating the pronounced efficiency loss accompanying spectral red-shifting into the deep-NIR region. This trend highlights the critical role of rational device design in mitigating EL efficiency degradation and underscores the necessity of jointly optimizing device architecture alongside molecular design for high-performance deep NIR TADF OLEDs.

3. Conclusion and outlook

In this review, we have summarized recent advances in deep-NIR TADF emitters, with a particular focus on molecular design strategies and their implications for OLED device performance. Current advances indicate that rational acceptor engineering—especially rigid and planar electron-withdrawing frameworks that preserve a twisted geometry with donor units—remains critical for achieving small ΔE_{ST} and suppressing non-radiative decay. Nevertheless, it should be noted that many reported "NIR" TADF systems primarily exhibit spectral tails extending into the NIR region rather than genuine NIR emission. Emitters with peak wavelengths exceeding 800 nm are still extremely scarce, and OLEDs based on such materials typically show modest EQEs, most commonly in the range of ~0. *x*% to 5%, with efficiency loss becoming more pronounced upon further red-shifting. These limitations currently hinder the practical application of NIR TADF OLEDs. In addition, the majority of reported NIR-TADF emitters rely heavily on TPA or its derivatives as donor units, while alternative donor scaffolds remain largely unexplored. This structural bias restricts molecular diversity and may further limit spectral extension and performance optimization.

Recent progress has validated several effective molecular design strategies, including the use of strong, compact acceptors such as pyrazine, benzo[*de*]anthracene-dicarbonitrile, and B–N multiple-resonance cores; π-conjugation extension and molecular rigidification to lower LUMO levels and suppress vibrational modes; and multi-acceptor or delocalized architectures that push emission further into the deep-NIR or NIR-II region. Nonetheless, the field continues to face fundamental challenges arising from the energy-gap law, enhanced vibronic coupling, large reorganization energies of CT states, and aggregation-induced quenching in solid films and practical device limitations including host–guest compatibility, charge balance, light extraction, and long-term stability.

Future research should focus on expanding donor diversity beyond TPA-type structures, developing compact and rigid donors with stronger electron-donating strength and better energy-level alignment to pair with high-performance acceptors. Simultaneously, introducing hybrid mechanisms such as MR and ESIPT may provide new ways to suppress high-frequency vibrational loss while retaining narrowband emission. Furthermore, improved control of aggregation through steric engineering and host–guest tuning, along with standardized evaluation of solid-state photophysical parameters (film PLQY, $\lambda_{max}/\lambda_{onset}$, ΔE_{ST}, and $k_r/k_{n,r}/k_{RISC}$), will enable better comparability across studies. On the device level, advances in solution-processable architectures, optimized doping ratios, and microcavity or tandem structures will further improve EQE and operational stability.

Overall, while the chemical feasibility of deep-NIR TADF emission has been clearly demonstrated, its practical realization—particularly in the NIR-II region—still faces pronounced device-level challenges. In addition to the intrinsic efficiency loss imposed by the energy gap law, NIR-II TADF OLEDs suffer from severe charge imbalance, inefficient exciton confinement, enhanced non-radiative decay, and aggravated exciton–polaron and exciton–exciton annihilation under electrical excitation. Moreover, limited optical outcoupling efficiency and accelerated device degradation caused by Joule heating further constrain the operational stability of long-wavelength devices. Addressing these unique challenges requires the synchronized optimization of molecular design, exciton management, and device engineering. Expanding the donor palette beyond TPA derivatives, together with advances in MR/ESIPT integration, aggregation control, and device architecture optimization, is expected to accelerate the development of efficient, stable, and manufacturable deep-NIR and NIR-II TADF OLEDs for next-generation optoelectronic technologies.

Author contributions

Z. R., J. L. and S. Y. initiated and supervised the project. S. L., X. Z., L. X. and C. Y. performed the literature survey and data collection. Z. R. and S. L. wrote the manuscript. All authors discussed the content and structure of the review and reviewed the final manuscript.

Conflicts of interest

There are no conflicts to declare.

Data availability

No primary research results, software or code have been included and no new data were generated or analysed as part of this review.

Acknowledgements

The financial support of the National Natural Science Foundation of China (No. 52273164 and 22575014), Beijing Natural Science Foundation (Z250016) and Shandong Provincial Natural Science Foundation (ZR2022ZD37) is gratefully acknowledged.

Notes and references

1 F. Nan, Z. Zhou, Q. Bai, K. Chen, Y. Liu and S. Wu, Sialic Acid-Modified NIR-II Fluorophore with Enhanced Brightness and Photoconversion Capability for Targeted Lymphoma Phototheranostics, *Anal. Chem.*, 2025, **97**(4), 2525–2536.

2 C. Si, A. K. Gupta, B. Basumatary, A. P. McKay, D. B. Cordes, A. M. Z. Slawin, I. D. W. Samuel and E. Zysman-Colman, Multi-Responsive Thermally Activated Delayed Fluorescence Materials: Optical $ZnCl_2$ Sensors and Efficient Green to Deep-Red OLEDs, *Adv. Funct. Mater.*, 2024, **34**, 2315935.

3 G. Ren, T. Pan, Y. Xu, J. Wang, L. Wang, R. Deng, S. Zhou, L. Tian, X. Wu and L. Zhou, Near-Infrared Ytterbium Complexes Based on Polycyclic Aromatic Dicarboxylate Ligands and the Solution-Processed NIR OLED with Irradiance up to 110,284 $\mu W/m^2$, *Inorg. Chem.*, 2025, **64**(16), 8343–8353.

4 H. Al-Sharji, R. Ilmi and M. S. Khan, Recent Progress in Phenoxazine-Based Thermally Activated Delayed Fluorescent Compounds and Their Full-Color Organic Light-Emitting Diodes, *Top. Curr. Chem.*, 2024, **382**(5), 5.

5 L. Ge, W. Zhang, Y.-H. Hao, M. Li, Y. Liu, M. Zhou and L.-S. Cui, Efficient and Stable Narrowband Pure-Red Light-Emitting Diodes with Electroluminescence Efficiencies Exceeding 43%, *J. Am. Chem. Soc.*, 2024, **146**(47), 32826–32836.

6 X. Qiu, A. Jung, A. Sevilla-Pym, P. Hu, S. Bräse and Z. M. Hudson, Glassy Organic Dots Exhibiting Near-Infrared TADF with Quantum Yields >40% for Cellular Imaging, *J. Mater. Chem. B*, 2025, **13**(41), 13282–13288.

7 H. C. Friedman, E. D. Cosco, T. L. Atallah, S. Jia, E. M. Sletten and J. R. Caram, Establishing Design Principles for Emissive Organic SWIR Chromophores from Energy Gap Laws, *Chem*, 2021, **7**(12), 3359–3376.

8 J. V. Caspar, E. M. Kober, B. P. Sullivan and T. J. Meyer, Application of the Energy Gap Law to the Decay of Charge-Transfer Excited States, *J. Am. Chem. Soc.*, 1982, **104**(2), 630–632.

9 Q. Sha, X. Li, X. Gu, T. Yuan and J. Hua, A Self-Aggregated Thermally Activated Delayed Fluorescence Nanoprobe for HClO Imaging and Activatable Photodynamic Therapy, *Talanta*, 2025, **286**, 127570.

10 S. Xu, Q. Zhang, X. Han, Y. Wang, X. Wang, M. Nazare, J.-D. Jiang and H.-Y. Hu, Dual-Mode Detection of Bacterial 16S Ribosomal RNA in Tissues, *ACS Sens.*, 2020, **5**(6), 1650–1656.

11 X. Li, G. Baryshnikov, C. Deng, X. Bao, B. Wu, Y. Zhou, H. Ågren and L. Zhu, A Three-Dimensional Ratiometric Sensing Strategy on Unimolecular Fluorescence–Thermally Activated Delayed Fluorescence Dual Emission, *Nat. Commun.*, 2019, **10**(1), 731.

12 J. Jin, H. Jiang, Q. Yang, L. Tang, Y. Tao, Y. Li, R. Chen, C. Zheng, Q. Fan, K. Y. Zhang, Q. Zhao and W. Huang, Thermally Activated Triplet Exciton Release for Highly Efficient Tri-Mode Organic Afterglow, *Nat. Commun.*, 2020, **11**(1), 842.

13 Q. Zhang, S. Xu, M. Li, Y. Wang, N. Zhang, Y. Guan, M. Chen, C.-F. Chen and H.-Y. Hu, Rationally Designed Organelle-Specific Thermally Activated Delayed Fluorescence Small Molecule Organic Probes for Time-Resolved Biological Applications, *Chem. Commun.*, 2019, **55**(39), 5639–5642.

14 Z. Zhu, D. Tian, P. Gao, K. Wang, Y. Li, X. Shu, J. Zhu and Q. Zhao, Cell-Penetrating Peptides Transport Noncovalently Linked Thermally Activated Delayed Fluorescence Nanoparticles for Time-Resolved Luminescence Imaging, *J. Am. Chem. Soc.*, 2018, **140**(50), 17484–17491.

15 F. Ni, Z. Zhu, X. Tong, W. Zeng, K. An, D. Wei, S. Gong, Q. Zhao, X. Zhou and C. Yang, Hydrophilic, Red-Emitting, and Thermally Activated Delayed Fluorescence Emitter for Time-Resolved Luminescence Imaging by Mitochondrion-Induced Aggregation in Living Cells, *Adv. Sci.*, 2019, **6**(5), 1801729.

16 J. R. Caine, P. Hu, A. T. Gogoulis and Z. M. Hudson, Unlocking New Applications for Thermally Activated Delayed Fluorescence Using Polymer Nanoparticles, *Acc. Mater. Res.*, 2023, **4**(10), 879–891.

17 H. Uoyama, K. Goushi, K. Shizu, H. Nomura and C. Adachi, Highly Efficient Organic Light-Emitting Diodes from Delayed Fluorescence, *Nature*, 2012, **492**(7428), 234–238.

18 H.-H. Cho, D. G. Congrave, S. Gorgon, V. Riesgo-Gonzalez, R. H. Friend and H. Bronstein, TADF Host Engineering for Improved Pure Blue Matrix-Free Hyperfluorescent OLEDs with Ultranarrow Emission, *Adv. Opt. Mater.*, 2025, **13**(23), 2500246.

19 B. Cui, J. Zhou, C. Duan and H. Xu, Blue Multiple-Resonance Thermally Activated Delayed Fluorescence Materials, *Adv. Opt. Mater.*, 2025, **13**(23), 2403295.
20 M. Li, L. Hua, J. Zhao, Y. Liu, S. Yan and Z. Ren, Regulating the Spatially Folded Arrangement of Donor and Acceptor Units To Achieve Efficient Orange-Red Thermally Activated Delayed Fluorescence, *Angew. Chem., Int. Ed.*, 2025, **64**(16), e202501179.
21 Q. Li, H. Zhao, M. Li, Y. Liu, S. Yan and Z. Ren, Fused Dual-Donor Design for Accelerating Reverse Intersystem Crossing Rates of Spatially Folded Through-Space Charge Transfer Emitters, *Angew. Chem., Int. Ed.*, 2025, **64**(26), e202506654.
22 Q. Li, H. Zhao, J. Zhao, Z. Cao, C. Yu, S. Yan and Z. Ren, Enhancing Electroluminescence Performance of Ultra-Deep-Blue Through-Space Charge Transfer Emitters with CIEy ≈ 0.05 via Methyl-Modification, *Chem. Sci.*, 2025, **16**(15), 6434–6442.
23 C. Jiang, Y. Nie, C. Cao, X. Song, J. Liang, X. Zhuang, Z. Li, B. Liang and Y. Wang, Sulfur-Embedded Pure Green Multiple Resonance TADF Emitters: Optimizing Photophysical and Electroluminescent Properties, *Adv. Sci.*, 2025, e12796.
24 S. Wu, D. Chen, X.-H. Zhang, D. Sun and E. Zysman-Colman, A Multiresonant Thermally Activated Delayed Fluorescent Dendrimer with Intramolecular Energy Transfer: Application for Efficient Host-Free Green Solution-Processed Organic Light-emitting Diodes, *Adv. Mater.*, 2025, **37**(8), 2415289.
25 Z. Yan, J. Lin, Q. Chen, X. Zhuang, L. Yuan, Z. Li, Z. Wang, Y.-X. Zheng, Y. Wang and H. Bi, Symmetric Multi-Resonant TADF Emitters via Chiral Space Conjugation Toward Strong Chiroptical Responses and Narrowband Green Circularly Polarized Electroluminescence, *Adv. Mater.*, 2025, e11230.
26 X. Liu, L. Hua, X. Lai, J. H. Kim, Q. Zhu, J. Y. Lee, W. Zhu and Y. Wang, High-Performance Solution Processable Red TADF-OLED with External Quantum Efficiency Exceeding 28% Using a Multi-Resonance Emitter Host, *Adv. Mater.*, 2025, **37**(21), 2500690.
27 H. Wang, S. Lin, J.-X. Chen, X.-Y. Hao, X.-C. Fan, Y.-Z. Shi, J. Yu, X.-K. Chen, K. Wang and X.-H. Zhang, Stepwise Planarizing Geometries of D–A Type Red Thermally Activated Delayed Fluorescence Molecules in Condensed States Toward High-Efficiency Red/NIR OLEDs, *Adv. Funct. Mater.*, 2025, **35**(23), 2420489.
28 Y. Xiao, H. Wang, Z. Xie, M. Shen, R. Huang, Y. Miao, G. Liu, T. Yu and W. Huang, NIR-TADF Emitters and OLEDs: Challenges, Progress, and Perspectives, *Chem. Sci.*, 2022, **13**(31), 8906–8923.
29 S. Ahadzadeh, S. Brebels, W. Maes and W. Deferme, Strategies for Advancing Near-Infrared Organic Light-Emitting Diodes: Innovations in Luminescent Materials, Device Architectures, Fabrication Methods, and Applications, *Adv. Funct. Mater.*, 2025, 2419599.
30 U. Balijapalli, R. Nagata, N. Yamada, H. Nakanotani, M. Tanaka, A. D'Aléo, V. Placide, M. Mamada, Y. Tsuchiya and C. Adachi, Highly Efficient Near-Infrared Electrofluorescence from a Thermally Activated Delayed Fluorescence Molecule, *Angew. Chem., Int. Ed.*, 2021, **60**(15), 8477–8482.
31 J.-W. Tai, Y. Tang, K. Zhang, C.-Z. Yang, Z.-H. Pan, Y.-C. Lin, Y.-W. Shih, C.-H. Chen, T.-L. Chiu, J.-H. Lee, C.-K. Wang, C.-C. Wu and J. Fan, 13.2% EQE Near-Infrared TADF OLED with Emission Peak at 761 nm, *Chem. Eng. J.*, 2023, **452**, 139534.
32 H. Wang, Y. Gao, J. Chen, X.-C. Fan, Y.-Z. Shi, J. Yu, K. Wang, S. Li, C.-S. Lee and X. Zhang, Versatile Thermally Activated Delayed Fluorescence Material Enabling High Efficiencies in both Photodynamic Therapy and Deep-Red/NIR Electroluminescence, *ACS Nano*, 2025, **19**(2), 2549–2558.
33 J. Jiang, Z. Xu, J. Zhou, M. Hanif, Q. Jiang, D. Hu, R. Zhao, C. Wang, L. Liu, D. Ma, Y. Ma and Y. Cao, Enhanced Pi Conjugation and Donor/Acceptor Interactions in D-A-D Type Emitter for Highly Efficient Near-Infrared Organic Light-Emitting Diodes with an Emission Peak at 840 nm, *Chem. Mater.*, 2019, **31**(17), 6499–6505.
34 J. Xu, X. Zheng, T.-B. Ren, L. Shi, X. Yin, L. Yuan and X.-B. Zhang, Recent Advances in Near-Infrared-II Organic J-Aggregates for Bio-Applications, *Coord. Chem. Rev.*, 2025, **528**, 216379.
35 T. Xu, J. Kong, Y. Chen, W. Cui, Y. Fang, W. Zhang, M. Wang, M. Zhou, Y. Li, R. Jin and Y. Song, Triple-Functional CuxAu61-x Nanoclusters with NIR-II Photoluminescence, Photothermal and Photodynamic Properties and Their Bio-Application, *Adv. Sci.*, 2025, **12**(39), e09283.
36 C. An, W. Deng, Y. Xie, K. An, H. Cao, D. Yang, Y. Chen, W. Liu, Y. Xu, N. Li, H. Wu and Y. Cao, Efficient Near-Infrared Organic Light-Emitting Diodes with Emission Peak Above 900 nm Enabled by Enhanced Photoluminescence Quantum Yields and Out-Coupling Efficiencies, *Adv. Funct. Mater.*, 2024, **34**(18), 2313353.
37 N. Yamada, H. Nakanotani, A. Takagi, M. Mamada, U. Balijapalli, T. Ichikawa, E. Hirata, S. Kaizu, A. Tanaka, K. Itonaga and C. Adachi, Three-Dimensional Sensing of Surfaces by Projection of Invisible Electroluminescence from Organic Light-Emitting Diodes, *Sci. Adv.*, 2024, **10**(1), eadj6583.
38 S. Ahadzadeh, S. Brebels, W. Maes and W. Deferme, Strategies for Advancing Near-Infrared Organic Light-Emitting Diodes: Innovations in Luminescent Materials, Device Architectures, Fabrication Methods, and Applications, *Adv. Funct. Mater.*, 2025, 2419599.
39 F. Zhu, Y. Gao and J. Qiu, A Nontoxic and Environmentally Friendly NIR-II Phosphor for Night Vision, Bio-Imaging, Large-Scale Detection, and Information Anti-Counterfeiting with High-Resolution Imaging, *Adv. Opt. Mater.*, 2025, **13**(20), 2500549.
40 W. Liu, W. Deng, W. Wang, H. Wu, C. Gao, Y. Xie, J. Zhao, X. Dong, Z. Zhao, Z. Zheng, Y. Chi, L. Duan, X. Zhan, Y. Zou, H. Wu, J. Peng and Y. Cao, Ultrahigh-Radiance Near-Infrared Organic Light-Emitting Diodes, *Nat. Photonics*, 2025, **19**(6), 650–657.
41 Y. Zhang, D. Zhang, T. Huang, A. J. Gillett, Y. Liu, D. Hu, L. Cui, Z. Bin, G. Li, J. Wei and L. Duan, Multi-Resonance

Deep-Red Emitters with Shallow Potential-Energy Surfaces to Surpass Energy-Gap Law, *Angew. Chem., Int. Ed.*, 2021, **60**(37), 20498–20503.

42 Y. Pu, Q. Jin, Y. Zhang, C. Li, L. Duan and Y. Wang, Sulfur-Locked Multiple Resonance Emitters for High Performance Orange-Red/Deep-Red OLEDs, *Nat. Commun.*, 2025, **16**(1), 332.

43 T. Fan, M. Du, X. Jia, L. Wang, Z. Yin, Y. Shu, Y. Zhang, J. Wei, D. Zhang and L. Duan, High-Efficiency Narrowband Multi-Resonance Emitter Fusing Indolocarbazole Donors for BT. 2020 Red Electroluminescence and Ultralong Operation Lifetime, *Adv. Mater.*, 2023, **35**(30), 2301018.

44 D. G. Congrave, B. H. Drummond, P. J. Conaghan, H. Francis, S. T. E. Jones, C. P. Grey, N. C. Greenham, D. Credgington and H. Bronstein, A Simple Molecular Design Strategy for Delayed Fluorescence toward 1000 nm, *J. Am. Chem. Soc.*, 2019, **141**(46), 18390–18394.

45 Q. Liang, J. Xu, J. Xue and J. Qiao, Near-Infrared-II Thermally Activated Delayed Fluorescence Organic Light-Emitting Diodes, *Chem. Commun.*, 2020, **56**(63), 8988–8991.

46 Y. Yu, H. Xing, D. Liu, M. Zhao, H. H.-Y. Sung, I. D. Williams, J. W. Y. Lam, G. Xie, Z. Zhao and B. Z. Tang, Solution-Processed AIEgen NIR OLEDs with EQE Approaching 15%, *Angew. Chem., Int. Ed.*, 2022, **134**(26), e202204279.

47 J.-X. Liang, Y. Tang, X. Wang, K. Zhang, Y.-W. Shih, C.-H. Chen, T.-L. Chiu, P. J. Li, J.-H. Lee, C.-K. Wang, C.-C. Wu and J. Fan, Highly Efficient Near-Infrared Thermally Activated Delayed Fluorescence Organic Light-Emitting Diodes with Emission Beyond 800 nm, *J. Mater. Chem. C*, 2023, **11**(21), 6981–6988.

48 H. Wang, K. Wang, J.-X. Chen, X. Zhang, L. Zhou, X.-C. Fan, Y.-C. Cheng, X.-Y. Hao, J. Yu and X.-H. Zhang, Enabling Record-high Deep-Red/Near-Infrared Electroluminescence Through Subtly Managing Intermolecular Interactions of a Thermally Activated Delayed Fluorescence Emitter, *Adv. Funct. Mater.*, 2023, **33**(41), 2304398.

49 J. Xu, J. Xue, Y. Dai, J. Zhang, J. Ren, C. Yao, S. Li, Q. Meng, X. Wen, H. Shao and J. Qiao, π-Bridge Mediated Coupling between Inter- and Intra-Molecular Charge Transfer in Aggregates for Highly Efficient Near-Infrared Emission, *Aggregate*, 2024, **5**(6), e634.

50 Y. Dai, J. Xu, X. Lei, Q.-Y. Meng and J. Qiao, Molecular Engineering of Donor/π-Bridge Enables High-Efficiency and Long-Lifetime Near-Infrared TADF-OLEDs, *Adv. Funct. Mater.*, 2025, **35**(2), 2412780.

51 S. Hu, Y. Li, K. Zhang, D.-Y. Zhou, L.-S. Liao and J. Fan, Pentacarbonitrile-Based Efficient Near-Infrared Thermally Activated Delayed Fluorescence OLEDs via Suppressing Excited-State Structural Relaxation, *J. Mater. Chem. C*, 2025, **13**(6), 2887–2894.

52 Z. Zhou, J. Pan, C. Guan, Y. Pu, J. Sun, J. Pan, W. Zhu and Y. Liu, Molecular Engineering Enables Efficient Thermally Activated Delayed Fluorescence Emitter Exceeding 1000 nm, *Chem. Eng. J.*, 2025, **523**, 168548.

53 H. Ye, D. H. Kim, X. Chen, A. S. D. Sandanayaka, J. U. Kim, E. Zaborova, G. Canard, Y. Tsuchiya, E. Y. Choi, J. W. Wu, F. Fages, J.-L. Bredas, A. D'Aléo, J.-C. Ribierre and C. Adachi, Near-Infrared Electroluminescence and Low Threshold Amplified Spontaneous Emission above 800 nm from a Thermally Activated Delayed Fluorescent Emitter, *Chem. Mater.*, 2018, **30**(19), 6702–6710.

54 J.-F. Cheng, Z.-H. Pan, K. Zhang, Y. Zhao, C.-K. Wang, L. Ding, M.-K. Fung and J. Fan, Interrupted Intramolecular Donor-Acceptor Interaction Compensated by Strong Through-Space Electronic Coupling for Highly Efficient Near-Infrared TADF with Emission over 800 nm, *Chem. Eng. J.*, 2022, **430**, 132744.

55 B. Ma, Z. Ding, D. Liu, Z. Zhou, K. Zhang, D. Dang, S. Zhang, S.-J. Su, W. Zhu and Y. Liu, A Feasible Strategy for a Highly Efficient Thermally Activated Delayed Fluorescence Emitter Over 900 nm Based on Phenalenone Derivatives, *Chem.–Eur. J.*, 2023, **29**(41), e202301197.

56 J. Xu, Y. Dai, J. Zhang, Z. Jia, Q. Meng and J. Qiao, Concerted Intramolecular and Intermolecular Charge Transfer for High-Efficiency Near-Infrared Thermally Activated Delayed Fluorescent Materials Approaching 900 nm, *Adv. Opt. Mater.*, 2024, **12**(3), 2300989.

57 R. Jiang, Z. Liu, T. Yang, D. Yang, D. Ma, B. Z. Tang and Z. Zhao, Tailored Near-Infrared Luminescent Materials with Fast Reverse Intersystem Crossing for Efficient Deep-Red/Near-Infrared Organic Light-Emitting Diodes with High Efficiencies and Small Roll-Offs, *Adv. Opt. Mater.*, 2024, **12**(9), 2302034.

58 A. D'Aléo, X. Tang, D.-H. Kim, D. Valverde, E. Zaborova, G. Canard, A. Brosseau, L. Mager, G. Clavier, C. Adachi, Y. Olivier and J.-C. Ribierre, Curcuminoid Derivatives with a Donor-Acceptor-Donor Architecture: An Outstanding Platform for Highly-Efficient Near-Infrared Electroluminescence and Amplified Spontaneous Emission, *Adv. Opt. Mater.*, 2025, **13**(20), 2500338.

59 Z.-L. Che, Y.-J. Yu, C.-C. Yan, S.-J. Ge, P. Zuo, J.-J. Wu, F.-M. Liu, Z.-Q. Feng, L.-S. Liao and X.-D. Wang, Advancing Beyond 800 Nm: Highly Stable Near-Infrared Thermally Activated Delayed Lasing Triggered by Excited-State Intramolecular Proton Transfer Process, *Adv. Mater.*, 2025, **37**(15), 2502129.

60 S. R. Sahoo, G. V. Baryshnikov and H. Ågren, Developing Red and Near-Infrared Delayed Fluorescence Emission in Nitrogen-Substituted Donor–Acceptor Polycyclic Hydrocarbon OLED Emitters: A Theoretical Study, *J. Phys. Chem. A*, 2025, **129**(10), 2396–2410.